Systematic coarse-grained modeling of complexation between small interfering RNA and polycations

Zonghui Wei[1] and Erik Luijten[1,2,3,4,a)]
[1]*Graduate Program in Applied Physics, Northwestern University, Evanston, Illinois 60208, USA*
[2]*Department of Materials Science and Engineering, Northwestern University, Evanston, Illinois 60208, USA*
[3]*Department of Engineering Sciences and Applied Mathematics, Northwestern University, Evanston, Illinois 60208, USA*
[4]*Department of Physics and Astronomy, Northwestern University, Evanston, Illinois 60208, USA*

(Received 28 September 2015; accepted 25 November 2015; published online 14 December 2015)

All-atom molecular dynamics simulations can provide insight into the properties of polymeric gene-delivery carriers by elucidating their interactions and detailed binding patterns with nucleic acids. However, to explore nanoparticle formation through complexation of these polymers and nucleic acids and study their behavior at experimentally relevant time and length scales, a reliable coarse-grained model is needed. Here, we systematically develop such a model for the complexation of small interfering RNA (siRNA) and grafted polyethyleneimine copolymers, a promising candidate for siRNA delivery. We compare the predictions of this model with all-atom simulations and demonstrate that it is capable of reproducing detailed binding patterns, charge characteristics, and water release kinetics. Since the coarse-grained model accelerates the simulations by one to two orders of magnitude, it will make it possible to quantitatively investigate nanoparticle formation involving multiple siRNA molecules and cationic copolymers. © *2015 AIP Publishing LLC*. [http://dx.doi.org/10.1063/1.4937384]

I. INTRODUCTION

Gene therapy, which involves the delivery of foreign genomic material into host cells, can be used to treat inherited disorders, cancer, and viral infections, among many others. One of the central challenges of gene therapy is the design of effective gene carriers. Non-viral gene delivery vectors, such as synthetic polymers, are promising systems that offer the advantage of low toxicity and cost, as well as ease of industrial production.[1–4] One of the most popular polymers used in gene delivery is the polycation polyethyleneimine (PEI), which has been developed over the past two decades for the successful delivery of nucleic acids such as plasmid DNA,[5] oligonucleotides,[6] and small interfering RNA (siRNA).[7] RNA interference (RNAi) using siRNA is a promising therapeutic strategy.[8–10] Protective carriers are needed to deliver siRNA to the target site to avoid degradation by nucleases, to facilitate cellular uptake, and so on. PEI appears to be a promising carrier, as it offers pH-buffering properties,[6] high affinity to siRNA,[11] high gene-delivery efficiency,[12,13] and the advantage of being easily modified with other functional groups.[14] In spite of this great potential, there exist several challenges that prevent the clinical use of such gene-delivery systems. For example, controlling the colloidal stability of nanoparticles created via self-assembly of DNA and PEI-based polymers poses a major challenge.[15,16] Furthermore, there is evidence that nanoparticle morphology plays an important role in dictating biofunctionality, including cellular and tissue uptake,[17,18] tissue diffusion,[19] and circulation stability.[20] In collaboration with Mao and co-workers, we previously reported effective shape control of plasmid DNA and polyphosphoramidate (PPA)-based nanoparticles[21,22] and showed that nanoparticle shape correlates with transfection efficiency. To achieve shape control for PEI/siRNA nanoparticles as well, new PEI-based carriers are needed. PEI copolymers have emerged as a promising candidate, but the multitude of parameters that needs to be examined provides a strong motivation to develop modeling techniques that guide the design of these PEI-based carriers. Here, we examine the systematic generation of coarse-grained (CG) models that offer such quantitative predictive capabilities.

All-atom (AA) molecular dynamics (MD) simulations have provided insight into the complexation of siRNA with PEI by elucidating the interaction of hyperbranched PEI (hyPEI) with a single siRNA molecule.[11] Sun *et al.* performed AA simulations involving multiple siRNA molecules to study the effect of lipid substitution on PEI-mediated siRNA complexation.[14] However, the time and length scales of the full siRNA/PEI complexation process, as well as the need to track shape fluctuations of the resulting nanoparticles, preclude the exclusive use of AA modeling. These limitations can be overcome by CG simulations based upon a bead–spring model, as employed in investigations on shape control of micellar DNA nanoparticles[21,22] and other coarse-grained studies of DNA condensation by polycations.[23–25] In such models, which often use an implicit solvent, the nucleic acids are represented as simple polyanions, which capture sufficient structural properties to provide mechanistic insights,

a)Author to whom correspondence should be addressed. Electronic mail: luijten@northwestern.edu

but lack the details that enable quantitative predictions of the binding pattern and dynamics. To remedy this, we employ atomistic input to develop a CG model that can achieve the experimentally relevant time and length scales, while partially retaining important atomistic information.

A CG force field that has been widely used and validated in the context of biological systems, in particular in simulations of lipids[26] and proteins,[27] is the MARTINI force field.[28] It is particularly interesting to examine its capabilities, since only very recently a DNA model was released employing this force field.[29] We investigate the extension of this model to siRNA, focusing on the representation with polarizable water[30] and full long-range electrostatic interactions, as those are crucial in the complexation of siRNA with PEI copolymers. For the latter, we choose polyethylene glycol (PEG)-grafted linear PEI, following our earlier work on DNA nanoparticle shape control.[21,22] Such copolymers are easier to synthesize and provide a larger parameter space for shape control than PEG/PEI block copolymers. We systematically develop a CG model for this polymer based upon AA simulations and also compare the results for siRNA–copolymer complexation obtained via these modeling strategies, with a particular emphasis on the role of PEG grafting density, one of the important parameters influencing the morphology of self-assembled DNA nanoparticles.[22] The CG force fields presented here will make it possible to perform greatly accelerated simulations of siRNA nanoparticle formation while retaining sufficient atomistic detail to provide quantitative input to future experiments.

II. METHODS AND MODELS

A. All-atom molecular dynamics simulations of PEG-grafted linear PEI

We develop an AA force field for PEG-grafted linear PEI (chemical structure shown in Fig. 1) based on the CHARMM General Force Field (CGenFF) version 2b8.[31] The corresponding CGenFF program[32,33] (version 0.9.7.1 beta) can automatically assign parameters to a compound by exploiting analogies to small molecules and accompanies these parameters with an evaluation of their accuracy expressed through a "penalty score." Thus, we employ the "divide-and-conquer" strategy, splitting the polymer into small building blocks and designing compounds containing

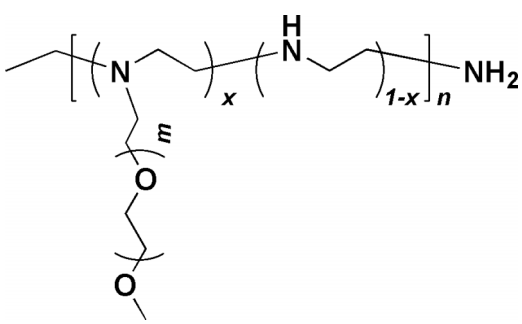

FIG. 1. Chemical structure of PEG-grafted PEI.

them based upon the local environment of individual residues within the polymer. These compounds are then evaluated in the CGenFF program to obtain an initial estimate of the force-field parameters. Parameters with low penalty scores are adopted directly for simulations. For the compounds we designed, all the partial charges and bond and angle parameters obtained by the CGenFF program show acceptable penalty scores (less than 50), whereas some dihedral parameters have high penalty scores. We choose to optimize these dihedral parameters *via* quantum-mechanical relaxed potential-energy surface scans using Gaussian09[34] with second-order Møller–Plesset perturbation theory (MP2) and the 6-31G(d) basis set. The Force Field Toolkit[35] implemented in Visual Molecular Dynamics (VMD)[36] is then used to fit these dihedral parameters by reproducing the quantum-mechanical potential energy surface using molecular mechanics. This parametrization strategy is more rigorous than earlier work,[37] where the force field was obtained by small-molecule analogy only, without further optimization based on quantum-mechanical calculations. Details of the parametrization of the PEG-grafted PEI AA force field are provided in the supplementary material.[38]

Considering the computational cost of AA simulations, we choose to simulate a linear PEI backbone of 50 amine groups and PEG grafts of 20 monomers each. This choice corresponds to PEI2.2k-*g*-PEG0.9k. The grafting density is defined as the number of grafted PEG chains divided by the number of amine groups in the PEI backbone. By varying the number of grafted chains, we simulate grafted copolymers with grafting density 0% (linear PEI backbone only), 2% (one PEG graft), 4%, and 8%. In view of the beneficial effect of low pH on siRNA delivery efficiency,[39] we adopt pH 2 for our systems. To represent this condition, 82% of the nitrogen sites in PEI backbone are protonated[40] (the charged sites are fixed during the simulation and distributed as illustrated in Sec. I in the supplementary material and Fig. S1[38]). Initial configurations for the polymer are generated by the VMD Psfgen plugin and then solvated into rectangular water boxes with a solvation shell of 16 Å thickness, which results in approximately ten thousand water molecules in each system. The size of the simulation cells and exact numbers of water molecules are listed in Table S3 in the supplementary material.[38] To neutralize the system, 41 Cl^- ions are added. After energy minimization for 5000 steps, each system is heated from 0 K to 300 K in 400 ps with an increase of 30 K after every 40 ps. Subsequently, these systems are equilibrated for 100 ns using Langevin dynamics as thermostat with a damping parameter of 5 ps^{-1} and Nosé–Hoover Langevin piston pressure control[41,42] with an oscillation time scale of 200 fs and a damping time scale of 100 fs to maintain a pressure of 1 bar. A production run of 200 ns is used for data analysis and serves as input for parametrization of the CG polycation model. In addition, the final configurations of each grafted PEI are used as the starting configurations for the complexation simulations described next.

All AA simulations are performed using the NAMD package[43] with the TIP3P[44] water model, periodic boundary conditions, and full electrostatics using the Particle–Mesh–Ewald (PME) method.[45] We use a time step of 2 fs and constrain all

bonds involving hydrogen atoms via the SHAKE algorithm.[46] A cutoff of 12 Å is set for the short-range interactions and the real-space contribution to the electrostatic calculations.

B. All-atom molecular dynamics simulations of siRNA complexation with PEG-grafted PEI

To examine complexation of grafted PEI-copolymers with siRNA, we construct siRNA composed of 50 nucleotides and with a net negative charge of −48 e in its fully deprotonated state,

sense strand: GAGCCCUUCUUUGACUCCCUGGUGA

antisense strand: UCACCAGGGAGUCAAAGAAGGG-CUC.

We use the Nucleic Acid Builder[47] via the make-na server (http://structure.usc.edu/make-na/) to build the initial configuration of the siRNA in the canonical A form and employ the CHARMM36 force field.[48,49] In constructing the initial configuration, which comprises two grafted PEI copolymers and one siRNA molecule, the centers of mass of the polycations and the siRNA form an equilateral triangle with side length 40 Å, aligned such that their principal axes are parallel and perpendicular to the plane of triangle. Then, the solute is solvated into a rectangular water box with a solvation shell of 17 Å thickness, which results in approximately 39 000–59 000 water molecules in each system. The size of the simulation cells and exact number of water molecules in each system are listed in Table S4 in the supplementary material.[38] 48 Na^+ ions and 82 Cl^- ions are added to the water box, serving as counterions to the siRNA and the polycations, respectively. After energy minimization for 5000 steps with the solute molecules fixed, followed by another 5000 steps unrestrained minimization, the systems are heated from 0 K to 300 K during 800 ps with an increase of 30 K after every 80 ps. The resulting configurations are simulated for 60 ns at 300 K and 1 bar using Langevin dynamics as thermostat and Nosé–Hoover Langevin piston pressure control, with the same damping parameter choices as in the AA simulations of isolated PEG-g-PEI in water. All other parameters of the simulation protocol also are chosen as described in Sec. II A.

C. Coarse-grained molecular dynamics simulations based on MARTINI force field

We employ the MARTINI force field for CG simulations of siRNA and grafted PEI. In view of the recent publication of a DNA model within the framework of this force field[29] and given the structural similarities between siRNA and a short DNA fragment in terms of their negatively charged anionic phosphodiester backbones, we represent siRNA by this model using double-stranded DNA in the canonical A form. In the DNA force field, the double-helical structure is imposed via an elastic network. This network comes in two variants, a "stiff network" that is better at retaining large-scale structures and a "soft network" that provides more realistic rotation of bases and a persistence length closer to experiment. We found that the soft elastic network is not strong enough to maintain the canonical A form very well, as illustrated in Fig. S8 in the supplementary material,[38] and thus use the stiff elastic network. Its main drawback is that a significantly increased persistence length is not expected to play a major role, given the short RNA length studied here.

TABLE I. MARTINI CG bead choice.

CG bead name	MARTINI bead type	Corresponding AA atom groups
u (neutral PEI bead)	SNda	$-CH_2NHCH_2-$
p (charged PEI bead)	SQd	$-CH_2NH_2^+CH_2-$
e1 (PEI left end bead)	Nda	$CH_3CH_2NHCH_2-$
e2 (PEI right end bead)	SQd	$-CH_2NH_3^+$
g (PEG bead)	SNa	$-CH_2OCH_2-$ or $-CH_2OCH_3$
l (PEI linking bead)	Na	$-CH_2NCH_2-$ | CH_2

Our model for grafted PEI is parametrized based upon the AA simulations of a single polymer chain in water (Sec. II A). Table I lists the choices for the MARTINI bead types. With the separations that we adopted, for most chemical groups, three heavy atoms are mapped on one CG bead, slightly more detailed than the 4-to-1 mapping typically employed in the MARTINI force field. These beads are assigned as smaller beads and labeled "S." Figure 2 shows an example structure of CG PEG-grafted PEI at grafting density 2%. Using the chosen mapping scheme, we then parametrize the CG bond, angle, and dihedral interaction coefficients by matching all the corresponding distributions (listed in Table S5 in the supplementary material[38]) with their counterparts extracted from the AA simulations. Details of this parametrization, the bonded force field parameters, and a comparison between AA and CG simulations of the radius of gyration of the polymer are provided in the supplementary material.[38] As electrostatic interactions are instrumental in the complexation of siRNA and polycations, we choose polarizable water model over the standard water model to achieve a more precise representation of local electrostatic screening. We observe that use of the standard water model will lead to compact polycation structures due to an overestimation of the attraction between ions and charged beads, as shown in Fig. S7[38] in the supplementary material.

Using these CG force fields, we perform complexation simulations. Two grafted PEI and one siRNA are placed in a similar initial configuration as in the AA simulations (Sec. II B), with the geometric centers of polycations and

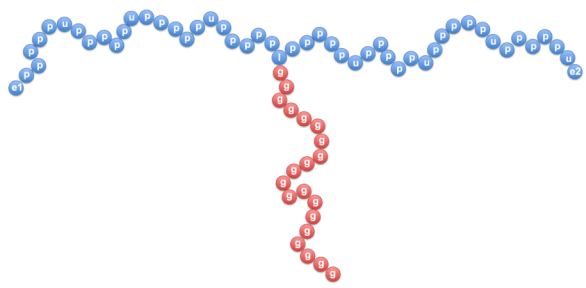

FIG. 2. CG representation of PEG-grafted PEI at grafting density 2%.

siRNA forming an equilateral triangle of side length 4 nm and the molecules aligned such that their principal axes are parallel to each other and perpendicular to the plane of the triangle. The solutes are placed in periodic cubic water boxes with side length 14 nm for grafting densities 0% and 2%, and side length 15 nm for grafting densities 4% and 8%. 48 Na^+ ions and 82 Cl^- ions are added to neutralize the charges on the siRNA and the polycations. After energy minimization using the steepest descent algorithm, each system is equilibrated with a time step of 1 fs for 4 ns and a time step of 3 fs for 18 ns. After equilibration, a production run of 100 ns is performed with a time step of 10 fs. The system is coupled to an isotropic Berendsen barostat[50] at pressure of 1 bar with a time constant of 4 ps. Grafted PEI, siRNA, and water are each thermostatted separately at a temperature of 300 K using stochastic velocity rescaling,[51] with a time constant of 1 ps. All CG simulations are performed with the GROMACS simulation package[52] (version 4.6.7). The Lennard-Jones interactions are smoothly shifted to zero between 0.9 and 1.2 nm via a polynomial such that the potential and its derivatives are continuous at the cutoff. As in the AA simulations, the electrostatic interactions are treated via PME. We employ a real-space cutoff of 1.2 nm and a spacing of the Fourier grid of 0.12 nm. The global relative dielectric constant is set to 2.5 which in conjunction with the polarizable water model produces realistic dielectric behavior.

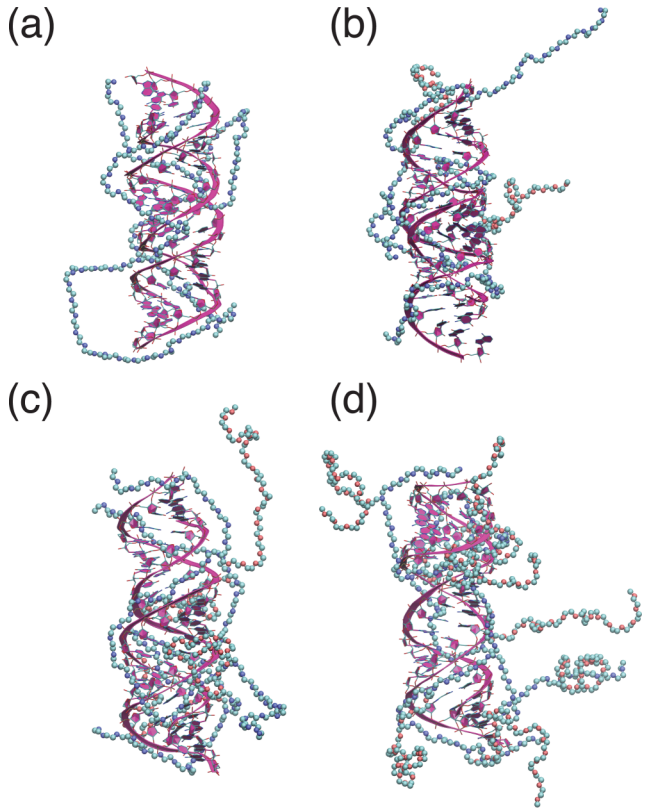

FIG. 3. Typical configurations of siRNA complexed with two PEG-grafted PEI chains at grafting density (a) 0%, (b) 2%, (c) 4%, and (d) 8%, obtained from AA simulations. Water molecules, ions, and hydrogen atoms are included in the simulations but not shown here for clarity. Color codes for the polymer chain: red–oxygen (PEG), blue–nitrogen (PEI), and cyan–carbon.

III. RESULTS AND DISCUSSION

A. Binding patterns

The binding between siRNA and PEI-based polymers depends on the structure of the PEI backbone and possible chemical modifications. Zheng *et al.* studied the binding of siRNA with hyPEI, which is a charged spherical polymer rather than a linear molecule. To increase its contact with the positively charged groups on the hyPEI, siRNA tends to adapt its structure in the form of local roll and tilt deformations.[11] Such strong siRNA-deforming characteristics upon condensation are frequently observed in condensation with highly branched polymers, such as dendrimers.[53–57] For binding with lower-generation dendrimers as well as certain polycations smaller in size than siRNA, such as low-molecular-weight linear or branched poly(L-lysine), Ouyang *et al.* have reported that polycations with lower total charge preferably bind within the major groove of siRNA, whereas those with higher total charge appear to bind less specifically on different regions of the siRNA.[53] Considering that linear PEI shows a better safety profile than branched PEI,[58,59] here we explore how linear PEI2.2k-*g*-PEG0.9k chains, which are longer than siRNA and far more flexible, bind to siRNA and how this condensation affects the siRNA structure.

Figure 3 shows the final configurations of the complexes formed at different PEG grafting densities, as obtained via the AA simulations described in Sec. II B. For both polymers present in the system, certain parts of the PEI backbones bind closely with the siRNA, exhibiting a tendency to wrap along the siRNA phosphate groups within the minor grooves, whereas other parts are located away from the siRNA. As expected, the PEG grafts, which do not experience the electrostatic interaction responsible for the complexation, tend to stay away from the siRNA.

To examine whether the CG model can reproduce this binding picture, Fig. 4 shows the final configurations of the CG simulations of Sec. II C. Qualitatively, the relative positions of the PEI backbones and the PEG grafts are similar to those observed in the AA simulations, with parts of the PEI backbones wrapping around the siRNA and the PEG grafts located away from the siRNA.

To quantify the locations of the PEI backbones and PEG grafts relative to the siRNA, we plot the cumulative percentage of the PEI nitrogen atoms and PEG oxygen atoms as a function of distance to any siRNA C1′ atom, averaged over the last 10 ns of each AA simulation (Fig. 5(a)) and the cumulative percentage of PEI beads and PEG beads as a function of distance to any siRNA BB3 bead, averaged over the last 20 ns of each CG simulation (Fig. 5(b)). The C1′ atoms reside on the sugar rings of the siRNA, located approximately 5 Å away from the surface of the helical "tube" defined by the phosphorus atoms. The BB3 beads are the CG beads representing the C3′, C2′, and C1′ atoms and corresponding hydrogen atoms in the sugar ring in the MARTINI model and are located nearly on the surface of the helical tube defined by the BB1 beads, which in turn are the CG representations for the phosphate groups. In both models, the cumulative

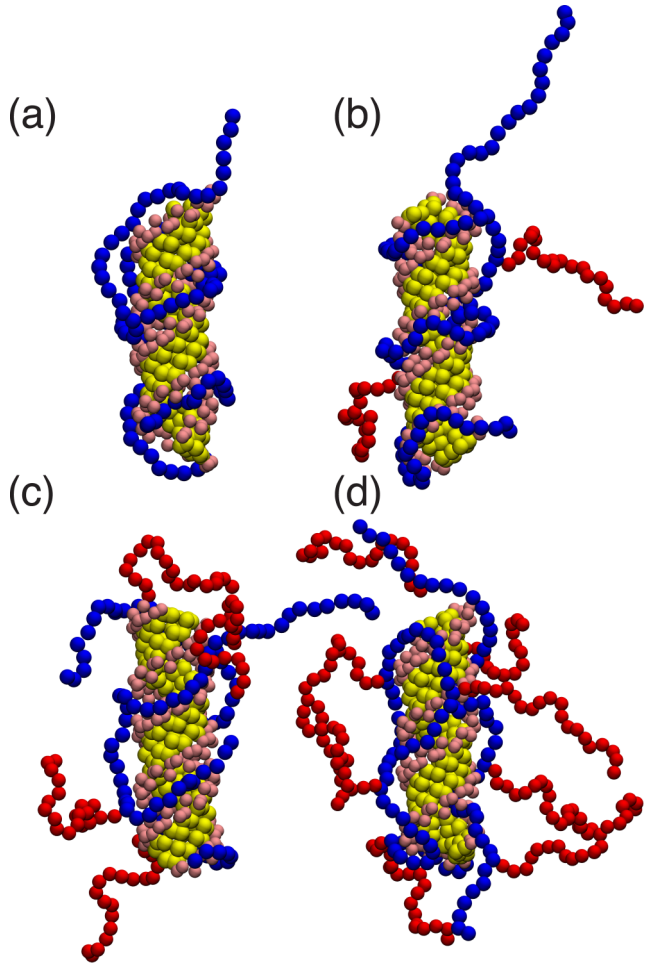

FIG. 4. Typical configurations of siRNA complexed with two PEG-grafted PEI chains at grafting density (a) 0%, (b) 2%, (c) 4%, and (d) 8% as obtained in CG simulations. Water molecules and ions are not shown for clarity. Color codes: blue–PEI, red–PEG, pink–siRNA backbone, and yellow–siRNA base.

percentage of PEI sites rises quickly from 0% at ~0.5 nm to 80% at ~1 nm. The curves for the PEG sites start also at ~0.5 nm, but reach 80% around 2.1 to 2.4 nm (depending on grafting density) in the AA simulations and around 2.5 to 3.0 nm in the CG simulations. This confirms the observations of Figs. 3 and 4 that siRNA interacts closely with the PEI backbone whereas the PEG grafts tend to be located outside the siRNA grooves. The PEI distributions do not exhibit a systematic dependence on PEG grafting density, neither in the AA nor in the CG simulations. The curves representing the PEG sites start at approximately the same minimal distance as the PEI curves—this simply arises from the fact the PEG is grafted to the PEI backbone—but then grows significantly slower, as expected for the less condensed nature of the PEG monomers. This distribution is a crucial ingredient for tuning and understanding the surface properties of nanoparticles formed through complexation and for controlling the nature of the aggregation process, in particular the number of siRNA molecules that will be present within a single nanoparticle.

To provide a detailed view of the interaction between the PEI backbone and siRNA, Fig. 6(a) shows the radial distribution functions of PEI nitrogen atoms around the siRNA backbone oxygen atoms and around the base nitrogen or oxygen atoms, as obtained in AA simulations. Figure 6(b) is the corresponding counterpart for CG simulations, showing the radial distribution functions for PEI beads around the BB1/BB2 beads in the siRNA backbone (which contain the oxygen atoms in the siRNA backbone) and around the base SC1/SC2/SC3/SC4 beads (which represent the nitrogen and oxygen atoms in the bases). Both models show a strong short-distance peak demonstrating that PEI interacts primarily with the siRNA backbone rather than its bases. For AA simulations, this peak is located around 0.27 nm (Fig. 6(a)), corresponding to the hydrogen bonding between PEI amine and oxygen in the backbone. In the CG simulations (Fig. 6(b)), this peak has shifted to ~0.46 nm, owing to the larger size of the CG beads (excluded-volume separation 0.43 nm or 0.47 nm, depending on the interaction). The secondary and tertiary peaks (at 0.5 nm and 0.7 nm) in the PEI distribution around the backbone in Fig. 6(a) arise from indirect interactions, such as water-mediated hydrogen bonding. In the CG simulations, only a secondary peak is present, near 0.8 nm. Despite these differences, we note that the CG model is able to reproduce the direct interaction between PEI and the siRNA backbone via hydrogen bonding as well as, to a lesser degree, the indirect interactions.

As mentioned above, siRNA can undergo significant structural changes upon complexation with branched PEI. To gain insight into the effect of linear PEI (which has a much lower bending rigidity) on the siRNA structure, we

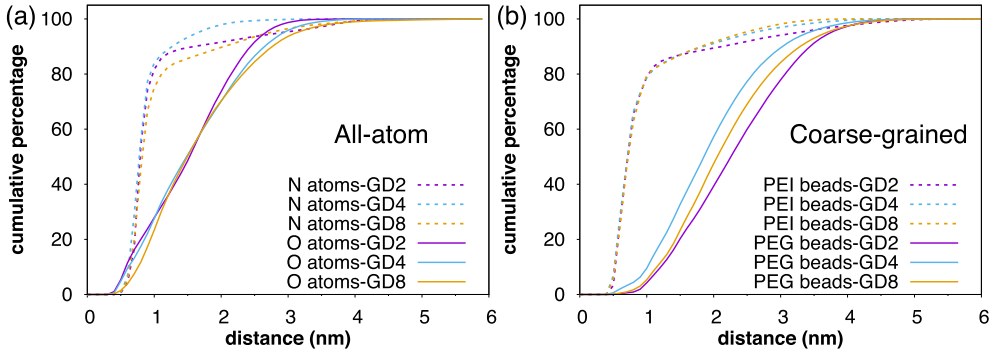

FIG. 5. Location of PEI backbones (dashed curves) and PEG grafts (solid lines) with respect to siRNA within a complex, as expressed via the cumulative percentage of PEI and PEG monomers from the siRNA backbone in (a) AA simulations and (b) CG simulations. In the AA simulations, PEI monomers are located via the nitrogen atoms and PEG monomers via the oxygen atoms, whereas in the CG simulations, the respective monomers are represented via single beads. All data are shown for PEG grafting densities 2%, 4%, and 8% (labeled GD2, GD4, and GD8).

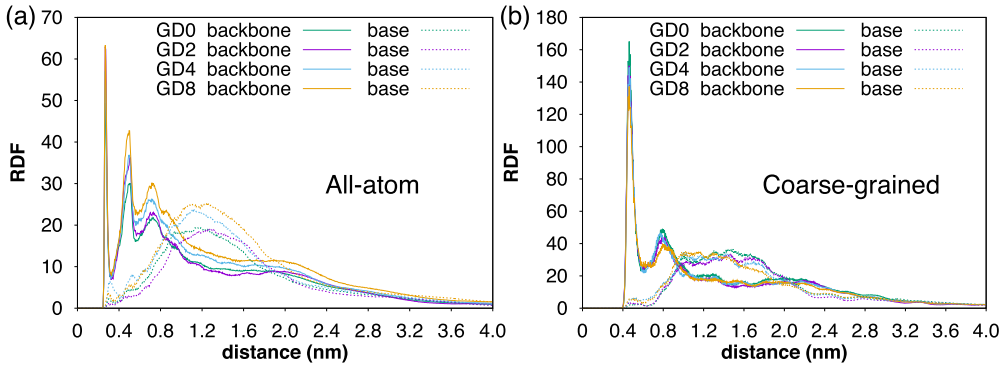

FIG. 6. Atom-level information of the interaction between PEI and siRNA via the radial distribution functions (RDF) of the PEI backbone sites around both the siRNA backbone and its bases in (a) AA simulations and (b) CG simulations. The CG simulations accurately reflect the direct hydrogen bonding between the PEI amines and the siRNA backbone (albeit with a shifted primary peak due to the bead size adopted in the MARTINI force field) rather than with the siRNA bases.

compare the shape of siRNA complexed with the polycations to that of isolated siRNA in water. We characterize the shape via the end-to-end distance along the principal axis of siRNA (Figs. 7(a) and 7(c)) and the cross-sectional area of siRNA (Figs. 7(b) and 7(d)). This area refers to the smallest rectangular box that encloses the siRNA, with the cross section oriented perpendicular to its principal axis. The length of the siRNA, as depicted in Fig. 7(a) for the last 20 ns of the AA simulations, decreases significantly upon binding, whereas the cross-sectional area (Fig. 7(b)) remains similar, indicating the absence of strong siRNA bending, which in turn justifies the use of the stiff elastic network. Interestingly, the shrinking along the principal axis can be directly related to the binding pattern, where the PEI backbones "wrap" around the siRNA phosphate groups on both strands within the minor grooves and then pulls these strands together via the strong electrostatic interactions (this is noticeable, e.g., in Fig. 3(b)). The absence of siRNA bending (as compared to complexation with hyperbranched PEI[11]) is easily understood from the very flexible nature of linear PEI backbone, which enables it to adapt its conformations during the binding process. As the PEG grafts tend to be located away from the siRNA, their presence does not have a strong effect on the siRNA shape.

The CG siRNA model cannot reproduce the subtle change of the end-to-end distance along the principal axis. As shown in Fig. 7(c), the end-to-end distance of siRNA in the complex is similar to or even a little larger than isolated siRNA in water and shows smaller fluctuations than in the AA simulations.

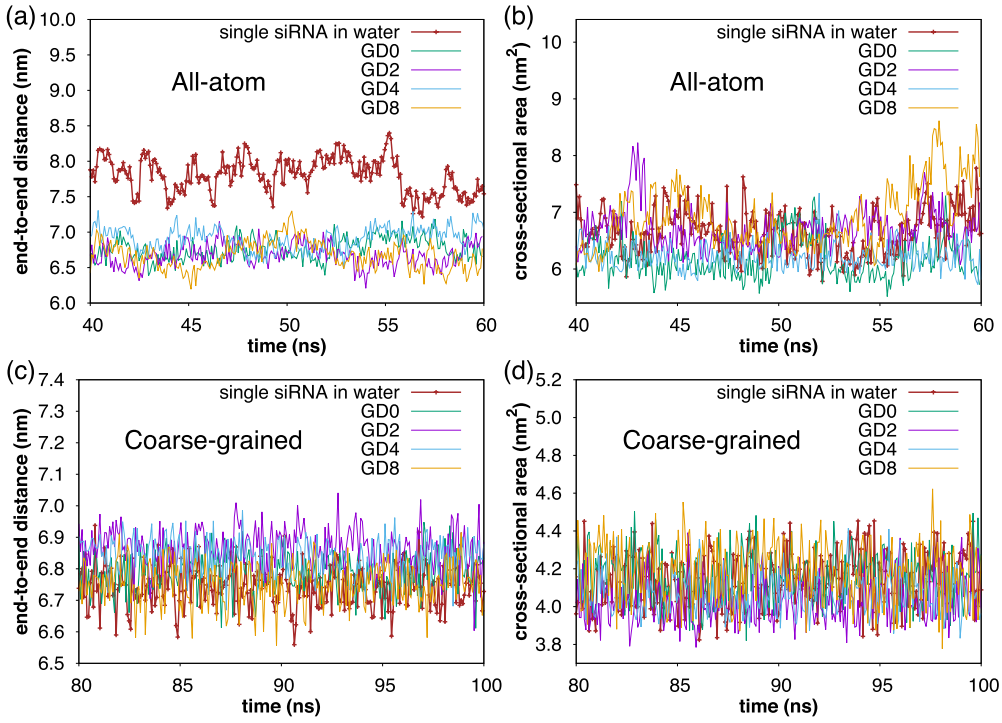

FIG. 7. Examination of potential siRNA shape change upon binding to grafted linear PEI. (a) The end-to-end distance along the principal axis of siRNA in AA simulations shows a significant length reduction, which arises from electrostatic interactions with PEI backbones located in the minor groove. (b) The cross-sectional area does not differ significantly between isolated and complexed siRNA, highlighting that PEI does not cause strong bending of siRNA. (c) The CG simulations cannot reproduce the length reduction but rather show an end-to-end distance that even has a slight *increase* upon binding with PEI. (d) The cross-sectional area in the CG simulations is independent of binding, as in the AA simulations, but significantly smaller.

The cross-sectional area also does not vary upon binding, which is consistent with the AA model. In an attempt to remedy this, we decreased the force constant in the stiff elastic network from the default value of 500 kJ mol^{-1} nm^{-2} to 300 kJ mol^{-1} nm^{-2} in intervals of 50 kJ mol^{-1} nm^{-2} and simulated isolated siRNA in water as well as siRNA complexation with grafted PEI at different grafting densities. However, none of these choices could reproduce the length reduction along the principal axis observed in the AA simulations, whereas in some of the simulations, the shape of the siRNA became unstable, as illustrated in Fig. S9 in the supplementary material.[38] In addition, we note that CG simulations of isolated siRNA in water already show a lower end-to-end distance (Fig. 7(c)) and cross-sectional area (Fig. 7(d)) than in the AA simulations. Potential causes for this discrepancy are the stiff elastic network that is used to retain the double-helical structure but can render the siRNA more compact, and the coarse-graining process itself, which groups several heavy atoms along with their linking hydrogen atoms into a single bead.

B. Charge neutralization

To investigate how the PEI backbones and ions in the solution neutralize the charge on siRNA, we plot the total charge of the polymers and ions as a function of distance to any siRNA C1′ atoms, averaged over the last 10 ns of the AA simulations (Fig. 8(a)) and the total charge as a function of distance to any siRNA BB1 beads, averaged over the last 20 ns of the CG simulations (Fig. 8(c)). These figures shows a clear "overcharging" peak,[23] where the net charge −48 e on the siRNA is neutralized by PEI and counterions located within 0.8 nm from the backbone, but the region in the next several nanometers from the backbone contains a net positive charge. These net-charge distributions are very similar for AA and CG simulations and in neither of the cases exhibit a strong dependence on grafting density. To elucidate the origin of the overcharging, we separate the net charge in contributions from ions and from protonated sites on the PEI (Fig. 8(b), AA simulations and Fig. 8(d), CG simulations). These figures show, again consistent between AA and CG simulations, that the monovalent ions do not play a role in the overcharging, but that this is wholly due to the connectivity of the PEI backbone, which forces excess charged groups to reside near the monomers that are condensed on the siRNA. These excess charges then influence the distribution of Cl^- ions, only followed at larger distances by the Na^+ counterions. The presence of PEG grafts does not interfere with the ability of PEI to neutralize the siRNA but causes a weak expansion of the ionic clouds in the AA simulations, which we ascribe to steric hindrance. Unlike the other features of the charge distributions, this last effect is not reflected in the CG simulations.

C. Water release

Water release is an important aspect of binding dynamics. Since water molecules adhering to macromolecules are less mobile, their release is associated with a gain in entropy.[60] We characterize this release by tracking the number of water molecules in the hydration shells of siRNA and the copolymers as binding takes place (Fig. 9). In the AA simulations

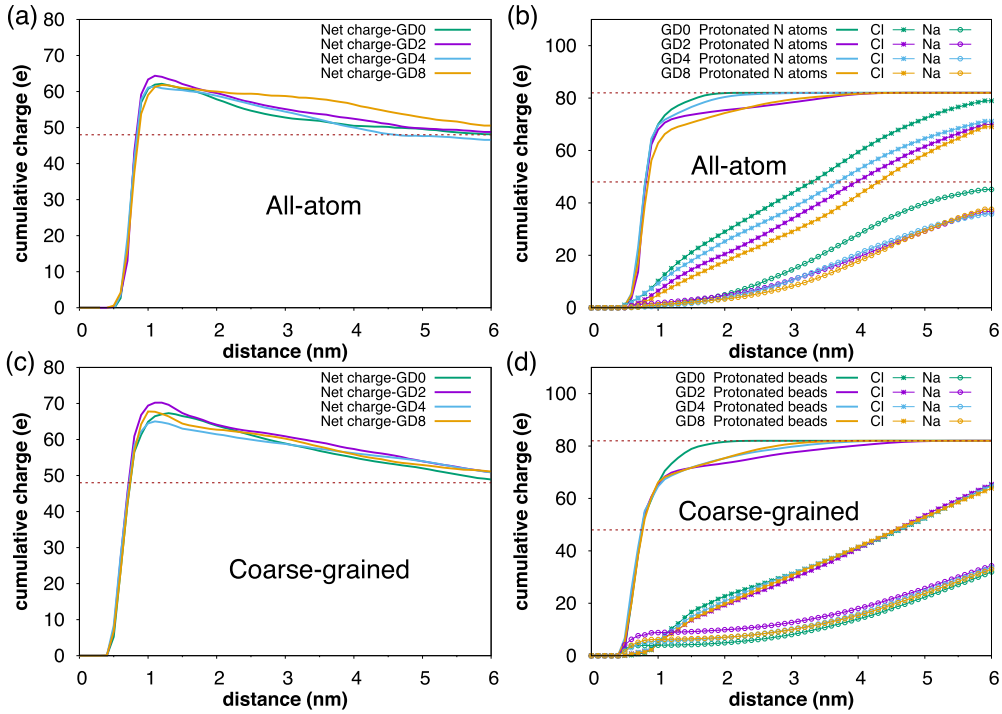

FIG. 8. Demonstration and origin of siRNA overcharging. Cumulative net charge around siRNA as calculated from the distance of charged groups and ions to (a) C1′ atoms in the AA simulations and (c) BB1 beads in the CG simulations shows an overcharging peak near 1.0 nm. The cumulative number of (b) protonated nitrogen (in PEI) and ions around siRNA in AA simulations and of (d) charged PEI beads and ions around siRNA in CG simulations shows that this overcharging is caused by PEI rather than by ions. The dashed horizontal lines correspond to the absolute net charge on either siRNA (48 e) or PEI (82 e).

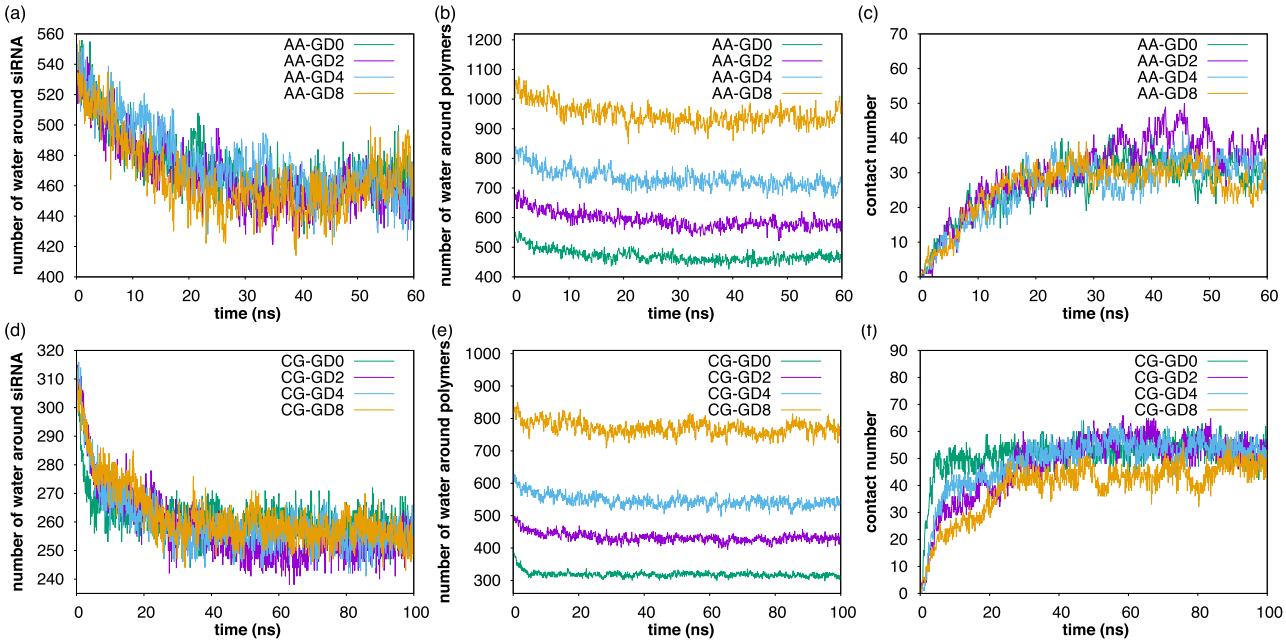

FIG. 9. Characterization of water release upon binding between siRNA and PEG-*g*-PEI copolymers. Top row (a)–(c): AA simulations. Bottom row (d)–(f): CG simulations. (a) and (d) Number of H_2O molecules around siRNA as a function of time; (b) and (e) number of H_2O molecules around copolymers as a function of time; (c) and (f) contact number between siRNA and copolymers as a function of time.

(Figs. 9(a) and 9(b)), a water molecule is considered part of the hydration shell if its oxygen atom is within 0.3 nm of siRNA or polymers. In the CG simulations (Figs. 9(d) and 9(e)), the W bead of polarizable water must be within 0.6 nm of siRNA or polymers. These hydration shell limits are chosen based upon the radial distribution functions of water molecules around siRNA and polymers (see Fig. S10[38] in the supplementary material). To correlate the reduction of the hydration shells with the binding process, we show the concomitant change in contact number in Figs. 9(c) and 9(f). In the AA simulations, PEI is considered in contact with siRNA if a nitrogen atom is within 0.3 nm of any siRNA nitrogen or oxygen atom. In the CG simulations, the contact criterion is a PEI bead within 0.6 nm of any siRNA bead. These criteria were adopted to include the regime of direct hydrogen bonding shown in Fig. 6. As illustrated in Figs. 9(c) and 9(f), within the first 30 ns of the simulations, the polymers move toward the siRNA. The relative change in the number of water molecules around siRNA is similar in the AA and CG simulations, and independent of PEG grafting density. On the other hand, the number of water molecules around the copolymers (Figs. 9(b) and 9(e)) is strongly dependent on grafting density, reflecting the hydrophilicity of PEG. Clearly, once multiple siRNA molecules are involved in aggregation, the PEG grafts may start to exert an important influence.

D. Discussion

The MARTINI model usually employs a 4-to-1 or 3-to-1 mapping of heavy atoms to a single bead. This mapping scheme is more refined than a typical bead–spring model, making it possible to retain some atomistic details in the parametrization of interaction coefficients based upon AA simulations. The model we present here based on the MARTINI force field successfully captures the general trend of siRNA and polycation binding, such as the binding structure and charge characteristics. In addition, the explicit solvent model adopted quite reasonably reproduces the water release from the hydration shells during complexation. Inevitably, certain details are lost in the coarse-graining process, including the contraction of siRNA along its main axis upon binding. In exchange for these trade-offs, the CG model offers an enormous acceleration compared to the AA simulations. Whereas 60 ns of the latter (using NAMD) take 60–90 days on 12 cores (Intel Xeon E5645, 2.40 GHz), the 100 ns CG simulations (using Gromacs) take only about 3 days on the same 12 cores (it is noteworthy that the Gromacs simulations were accelerated by approximately a factor 3 if three of these cores were dedicated to multithreaded PME calculation; moreover, Gromacs may have an intrinsically better performance than NAMD, as indicated in test simulations of DHFR in water[52]). We note that the use of a polarizable water model adds significantly to the computational cost, with a slow-down by approximately a factor of 3 for a pure water system.[30] When comparing AA and CG time scales, it is sometimes claimed that the standard MARTINI force field accelerates time fourfold.[28] Comparing the contacting dynamics in Figs. 9(c) and 9(f), we note that it takes about 30 ns for the AA simulations to reach a stable state, whereas this takes 10 to 30 ns for the CG simulations, starting from similar initial configurations. Thus, we cannot confirm that the factor 4 acceleration fully applies to our model. However, despite this, the sheer reduction in the number of particles due to the coarse-graining shown in Table II, as well as the larger time step (10 fs in the CG simulations compared to 2 fs in the AA simulations) due to the smoothening of the energy landscape, results in an acceleration that brings the investigation of siRNA nanoparticle formation through

TABLE II. Comparison of the number of atoms/beads in AA and CG complexation simulations.

Grafting density (%)	siRNA		PEG-grafted PEI		Water	
	AA	CG	AA	CG	AA	CG
0	1601	323	886	100	116 985	69 021
2	1601	323	1172	140	119 157	68 955
4	1601	323	1458	180	137 844	68 889
8	1601	323	2030	260	176 850	68 742

self-assembly within reach. Finally, we note that in some of our CG simulations, the contact number has not reached a plateau after more than 100 ns, indicating that the system has not reached a steady state yet. We attribute this to the strong electrostatic interactions between PEI and siRNA, which can cause the configuration to become trapped in metastable bound states.

E. Conclusion

We have developed a coarse-grained system of siRNA and PEG-grafted PEI within the MARTINI framework and evaluated its performance by comparing with atomistic simulations. To our knowledge, this is the first use of the MARTINI model for such a gene-delivery system. We demonstrated how PEG-*g*-PEI copolymers bind to siRNA and investigated the role of water in the complexation process, as well as the effect of PEG grafting density. In general, the coarse-grained model provides a reliable description of the binding process, capturing significant molecular detail while accelerating the simulations by one to two orders of magnitude. This illustrates the potential of coarse-grained simulations for the investigation of nanoparticle formation by multiple siRNA molecules and cationic copolymers.

ACKNOWLEDGMENTS

This research was supported through Award No. 70NANB14H012 from the U.S. Department of Commerce, National Institute of Standards and Technology, as part of the Center for Hierarchical Materials Design (CHiMaD) and through the National Institutes of Health through Grant Nos. R21 EB013274 and 1R01 EB018358-01A1. We thank the Quest high-performance computing facility at Northwestern University for computational resources. We also wish to thank Jaakko J. Uusitalo for helpful discussions on the MARTINI DNA model, Christopher G. Mayne, Josh Vermaas, James Gumbart, and Emad Tajkhorshid for discussions on the Force Field Toolkit, Tian Tang for correspondence regarding the AA force-field development for PEI, and Hai-Quan Mao, Yong Ren, and John-Michael Williford for discussions on experimental aspects of siRNA–polycation complexation.

[1]F. D. Ledley, Hum. Gene Ther. **6**, 1129–1144 (1995).
[2]C. P. Lollo, M. G. Banaszczyk, and H. C. Chiou, Curr. Opin. Mol. Ther. **2**, 136–142 (2000).
[3]S. Y. Wong, J. M. Pelet, and D. Putnam, Prog. Polym. Sci. **32**, 799–837 (2007).
[4]Y. Zhang, A. Satterlee, and L. Huang, Mol. Ther. **20**, 1298–1304 (2012).
[5]W. T. Godbey, K. K. Wu, and A. G. Mikos, J. Controlled Release **60**, 149–160 (1999).
[6]O. Boussif, F. Lezoualch, M. A. Zanta, M. D. Mergny, D. Scherman, B. Demeneix, and J. P. Behr, Proc. Natl. Acad. Sci. U. S. A. **92**, 7297–7301 (1995).
[7]B. Urban-Klein, S. Werth, S. Abuharbeid, F. Czubayko, and A. Aigner, Gene Ther. **12**, 461–466 (2005).
[8]D. Castanotto and J. J. Rossi, Nature **457**, 426–433 (2009).
[9]K. A. Afonin, W. W. Grabow, F. M. Walker, E. Bindewald, M. A. Dobrovolskaia, B. A. Shapiro, and L. Jaeger, Nat. Protoc. **6**, 2022–2034 (2011).
[10]R. Kole, A. R. Krainer, and S. Altman, Nat. Rev. Drug Discovery **11**, 125–140 (2012).
[11]M. Zheng, G. M. Pavan, M. Neeb, A. K. Schaper, A. Danani, G. Klebe, O. M. Merkel, and T. Kissel, ACS Nano **6**, 9447–9454 (2012).
[12]D. Jere, H. L. Jiang, R. Arote, Y. K. Kim, Y. J. Choi, M. H. Cho, T. Akaike, and C. S. Chot, Expert Opin. Drug Delivery **6**, 827–834 (2009).
[13]S. Patnaik and K. C. Gupta, Expert Opin. Drug Delivery **10**, 215–228 (2013).
[14]C. Sun, T. Tang, and H. Uludag, Biomaterials **34**, 2822–2833 (2013).
[15]R. S. Burke and S. H. Pun, Bioconjugate Chem. **19**, 693–704 (2008).
[16]M. J. Tiera, Q. Shi, F. M. Winnik, and J. C. Fernandes, Curr. Gene Ther. **11**, 288–306 (2011).
[17]B. D. Chithrani, A. A. Ghazani, and W. C. W. Chan, Nano Lett. **6**, 662–668 (2006).
[18]Arnida, M. M. Janat-Amsbury, A. Ray, C. M. Peterson, and H. Ghandehari, Eur. J. Pharm. Biopharm. **77**, 417–423 (2011).
[19]V. P. Chauhan, Z. Popovic, O. Chen, J. Cui, D. Fukumura, M. G. Bawendi, and R. K. Jain, Angew. Chem., Int. Ed. **50**, 11417–11420 (2011).
[20]Y. Geng, P. Dalhaimer, S. Cai, R. Tsai, M. Tewari, T. Minko, and D. E. Discher, Nat. Nanotechnol. **2**, 249–255 (2007).
[21]X. Jiang, W. Qu, D. Pan, Y. Ren, J. M. Williford, H. Cui, E. Luijten, and H. Q. Mao, Adv. Mater. **25**, 227–232 (2013).
[22]Z. Wei, Y. Ren, J. M. Williford, W. Qu, K. Huang, S. Ng, H. Q. Mao, and E. Luijten, ACS Biomater. Sci. Eng. **1**, 448–455 (2015).
[23]P. Y. Hsiao and E. Luijten, Phys. Rev. Lett. **97**, 148301 (2006).
[24]C. F. Narambuena, E. P. M. Leiva, M. Chavez-Paez, and E. Perez, Polymer **51**, 3293–3302 (2010).
[25]J. Ziebarth and Y. M. Wang, J. Phys. Chem. B **114**, 6225–6232 (2010).
[26]S. Esteban-Martin, H. J. Risselada, J. Salgado, and S. J. Marrink, J. Am. Chem. Soc. **131**, 15194–15202 (2009).
[27]P. J. Bond, J. Holyoake, A. Ivetac, S. Khalid, and M. S. P. Sansom, J. Struct. Biol. **157**, 593–605 (2007).
[28]S. J. Marrink, H. J. Risselada, S. Yefimov, D. P. Tieleman, and A. H. de Vries, J. Phys. Chem. B **111**, 7812–7824 (2007).
[29]J. J. Uusitalo, H. I. Ingólfsson, P. Akhshi, D. P. Tieleman, and S. J. Marrink, J. Chem. Theory Comput. **11**, 3932–3945 (2015).
[30]S. O. Yesylevskyy, L. V. Schafer, D. Sengupta, and S. J. Marrink, PLoS Comput. Biol. **6**, e1000810 (2010).
[31]K. Vanommeslaeghe, E. Hatcher, C. Acharya, S. Kundu, S. Zhong, J. Shim, E. Darian, O. Guvench, P. Lopes, I. Vorobyov, and A. D. Mackerell, Jr., J. Comput. Chem. **31**, 671–690 (2010).
[32]K. Vanommeslaeghe and A. D. MacKerell, Jr., J. Chem. Inf. Model. **52**, 3144–3154 (2012).
[33]K. Vanommeslaeghe, E. P. Raman, and A. D. MacKerell, Jr., J. Chem. Inf. Model. **52**, 3155–3168 (2012).
[34]M. J. Frisch, G. W. Trucks, H. B. Schlegel, G. E. Scuseria, M. A. Robb, J. R. Cheeseman, G. Scalmani, V. Barone, B. Mennucci, G. A. Petersson, H. Nakatsuji, M. Caricato, X. Li, H. P. Hratchian, A. F. Izmaylov, J. Bloino, G. Zheng, J. L. Sonnenberg, M. Hada, M. Ehara, K. Toyota, R. Fukuda, J. Hasegawa, M. Ishida, T. Nakajima, Y. Honda, O. Kitao, H. Nakai, T. Vreven, J. A. Montgomery, Jr., J. E. Peralta, F. Ogliaro, M. Bearpark, J. J. Heyd, E. Brothers, K. N. Kudin, V. N. Staroverov, R. Kobayashi, J. Normand, K. Raghavachari, A. Rendell, J. C. Burant, S. S. Iyengar, J. Tomasi, M. Cossi, N. Rega, J. M. Millam, M. Klene, J. E. Knox, J. B. Cross, V. Bakken, C. Adamo, J. Jaramillo, R. Gomperts, R. E. Stratmann, O. Yazyev, A. J. Austin, R. Cammi, C. Pomelli, J. W. Ochterski, R. L. Martin, K. Morokuma, V. G. Zakrzewski, G. A. Voth, P. Salvador, J. J. Dannenberg, S. Dapprich, A. D. Daniels, Ö. Farkas, J. B. Foresman, J. V. Ortiz, J. Cioslowski, and D. J. Fox, GAUSSIAN 09, Revision D.01, Gaussian, Inc., Wallingford, CT, 2009.
[35]C. G. Mayne, J. Saam, K. Schulten, E. Tajkhorshid, and J. C. Gumbart, J. Comput. Chem. **34**, 2757–2770 (2013).
[36]W. Humphrey, A. Dalke, and K. Schulten, J. Mol. Graphics **14**, 33–38 (1996).
[37]C. B. Sun, T. Tang, H. Uludag, and J. E. Cuervo, Biophys. J. **100**, 2754–2763 (2011).

[38]See supplementary material at http://dx.doi.org/10.1063/1.4937384 for details of parametrization of the PEG-grafted PEI AA force field, dimensions of the simulation cells in the AA simulations, details concerning the parametrization of the CG force field of PEG-grafted PEI within the MARTINI framework, tests on the soft and stiff elastic network of the MARTINI DNA model, and radial distribution functions of water molecules around siRNA or PEI.
[39]G. M. Pavan, S. Monteagudo, J. Guerra, B. Carrion, V. Ocana, J. Rodriguez-Lopez, A. Danani, F. C. Perez-Martinez, and V. Cena, Curr. Med. Chem. **19**, 4929–4941 (2012).
[40]G. M. Lindquist and R. A. Stratton, J. Colloid Interface Sci. **55**, 45–59 (1976).
[41]G. J. Martyna, D. J. Tobias, and M. L. Klein, J. Chem. Phys. **101**, 4177–4189 (1994).
[42]S. E. Feller, Y. H. Zhang, R. W. Pastor, and B. R. Brooks, J. Chem. Phys. **103**, 4613–4621 (1995).
[43]J. C. Phillips, R. Braun, W. Wang, J. Gumbart, E. Tajkhorshid, E. Villa, C. Chipot, R. D. Skeel, L. Kale, and K. Schulten, J. Comput. Chem. **26**, 1781–1802 (2005).
[44]W. L. Jorgensen, J. Am. Chem. Soc. **103**, 4721–4726 (1981).
[45]T. Darden, D. York, and L. Pedersen, J. Chem. Phys. **98**, 10089–10092 (1993).
[46]J. P. Ryckaert, G. Ciccotti, and H. J. C. Berendsen, J. Comput. Phys. **23**, 327–341 (1977).
[47]D. A. Case, J. T. Berryman, R. M. Betz, D. S. Cerutti, T. E. Cheatham III, T. A. Darden, R. E. Duke, T. J. Giese, H. Gohlke, A. W. Goetz, N. Homeyer, S. Izadi, P. Janowski, J. Kaus, A. Kovalenko, T. S. Lee, S. LeGrand, P. Li, T. Luchko, R. Luo, B. Madej, K. M. Merz, G. Monard, P. Needham, H. Nguyen, H. T. Nguyen, I. Omelyan, A. Onufriev, D. R. Roe, A. Roitberg, R. Salomon-Ferrer, C. L. Simmerling, W. Smith, J. Swails, R. C. Walker, J. Wang, R. M. Wolf, X. Wu, D. M. York, and P. A. Kollman, AMBER 2015, University of California, San Francisco, 2015.
[48]N. Foloppe and A. D. MacKerell, J. Comput. Chem. **21**, 86–104 (2000).
[49]A. D. MacKerell and N. K. Banavali, J. Comput. Chem. **21**, 105–120 (2000).
[50]H. J. C. Berendsen, J. P. M. Postma, W. F. Vangunsteren, A. Dinola, and J. R. Haak, J. Chem. Phys. **81**, 3684–3690 (1984).
[51]G. Bussi, D. Donadio, and M. Parrinello, J. Chem. Phys. **126**, 014101 (2007).
[52]B. Hess, C. Kutzner, D. van der Spoel, and E. Lindahl, J. Chem. Theory Comput. **4**, 435–447 (2008).
[53]D. Ouyang, H. Zhang, D. P. Herten, H. S. Parekh, and S. C. Smith, J. Phys. Chem. B **114**, 9220–9230 (2010).
[54]V. Vasumathi and P. K. Maiti, Macromolecules **43**, 8264–8274 (2010).
[55]O. M. Merkel, M. Zheng, M. A. Mintzer, G. M. Pavan, D. Librizzi, M. Maly, H. Hoffken, A. Danani, E. E. Simanek, and T. Kissel, J. Controlled Release **153**, 23–33 (2011).
[56]D. Ouyang, H. Zhang, H. S. Parekh, and S. C. Smith, Biophys. Chem. **158**, 126–133 (2011).
[57]K. Karatasos, P. Posocco, E. Laurini, and S. Pricl, Macromol. Biosci. **12**, 225–240 (2012).
[58]L. Wightman, R. Kircheis, V. Rossler, S. Carotta, R. Ruzicka, M. Kursa, and E. Wagner, J. Gene Med. **3**, 362–372 (2001).
[59]L. Buscail, B. Bournet, F. Vernejoul, G. Cambois, H. Lulka, N. Hanoun, M. Dufresne, A. Meulle, A. Vignolle-Vidoni, L. Ligat, N. Saint-Laurent, F. Pont, S. Dejean, M. Gayral, F. Martins, J. Torrisani, O. Barbey, F. Gross, R. Guimbaud, P. Otal, F. Lopez, G. Tiraby, and P. Cordelier, Mol. Ther. **23**, 779–789 (2015).
[60]J. D. Dunitz, Science **264**, 670 (1994).